Atmos. Chem. Phys. Discuss., 13, 20961–21002, 2013
www.atmos-chem-phys-discuss.net/13/20961/2013/
doi:10.5194/acpd-13-20961-2013

Atmospheric Chemistry and Physics Discussions

Similarities and differences of aerosol optical properties between southern and northern slopes of the Himalayas

C. Xu[1,2,3], Y. M. Ma[1,3], K. Yang[1], Z. K. Zhu[1,2,3,4], J. M. Wang[4], P. M. Amatya[1,2], and L. Zhao[1,2]

[1]Key Laboratory of Tibetan Environment Changes and Land Surface Processes, Institute of Tibetan Plateau Research, Chinese Academy of Sciences, Beijing 100101, China
[2]University of Chinese Academy of Sciences, Beijing 100049, China
[3]Qomolangma Station for Atmospheric Environmental Observation and Research, Chinese Academy of Sciences, Dingri 858200, Tibet, China
[4]Cold and Arid Regions Environmental and Engineering Research Institute, Chinese Academy of Sciences, Lanzhou 730000, China

Received: 27 May 2013 – Accepted: 29 July 2013 – Published: 13 August 2013

Correspondence to: Y. M. Ma (ymma@itpcas.ac.cn)

Published by Copernicus Publications on behalf of the European Geosciences Union.

Abstract

The Himalayas is located at the southern edge of the Tibetan Plateau, and it acts as a natural barrier for the transport of atmospheric aerosols, e.g. from the polluted regions of South Asia to the main body of the Tibetan Plateau. In this study, we investigate the seasonal and diurnal variations of aerosol optical properties measured at the three Aerosol Robotic Network (AERONET) sites over the southern (Pokhara station and EVK2-CNR station in Nepal) and northern (Qomolangma (Mt. Everest) station for Atmospheric and Environmental Observation and Research, Chinese Academy of Sciences (QOMS_CAS) in Tibet, China) slopes of the Himalayas. While observations at QOMS_CAS and EVK2-CNR can generally be representative of a remote background atmosphere, Pokhara is an urban site with much higher aerosol load due to the influence of local anthropogenic activities. The annual mean of aerosol optical depth (AOD) during the investigated period was 0.06 at QOMS_CAS, 0.04 at EVK2-CNR and 0.51 at Pokhara, respectively. Seasonal variations of aerosols are profoundly affected by large scale atmospheric circulation. Vegetation fires, peaking during April in the Himalayan region and northern India, contribute to a growing fine mode AOD at 500 nm at the three stations. Dust transported to these sites results in an increase of coarse mode AOD during the monsoon season at the three sites. Meanwhile, coarse mode AOD at EVK2-CNR is higher than QOMS_CAS from July to September, indicating the Himalayas blocks the coarse particles carried by the southwest winds. The precipitation scavenging effect is obvious at Pokhara, which can significantly reduce the aerosol load during the monsoon season. Unlike the seasonal variations, diurnal variations are mainly influenced by meso-scale systems and local topography. In general, precipitation can lead to a decrease of the aerosol load and the average particle size at each station. AOD changes in a short time with the emission rate near the emission source at Pokhara, while does not at the other two stations in remote regions. AOD increases during daytime due to the valley winds at EVK2-CNR, while this diurnal variation of AOD is absent at the other two stations. The surface heating influences the local con-

ACPD
13, 20961–21002, 2013

vection, which further controls the vertical aerosol exchange and the diffusion rate of pollutions to the surrounding areas. The Himalayas blocks most of the coarse particles across the mountains. Fine and coarse mode particles are mixed to make atmospheric composition more complex on the southern slope in spring, which leads to the greater inter-annual difference in diurnal cycles of Ångström exponent (AE) at EVK2-CNR than that at QOMS_CAS.

1 Introduction

Atmospheric aerosol effect is one of the largest uncertainties to predict climate change for inadequate understanding of its properties (IPCC, 2007), especially for anthropogenic aerosols (Kaufman et al., 2002). On one hand, aerosols absorbing and scattering solar radiation can change atmospheric temperature profile, surface solar radiation and reflected solar radiation at the top of atmosphere (Wild, 2009; Sena et al., 2013). On the other hand, aerosols can also act as cloud condensation nuclei (CCN) to impact cloud cover, cloud properties and precipitation, and ultimately influence the hydrological cycle (Ramanathan et al., 2001). Therefore, it is important to simulate and quantify climatic effects of atmospheric aerosols.

The studies of tropospheric aerosols and their impacts are of great importance (Li et al., 2011). Tibetan Plateau (TP) is the largest and highest plateau on the earth. TP acts as a receptor of natural and anthropogenic aerosols from the surrounding areas, and its environment is highly sensitive to climate change and human activities. The Himalayas is located at the southern edge of TP, and it acts as a natural barrier for the transport of atmospheric aerosols. However, the knowledge for aerosol optical properties is lacking on the TP.

Many studies have focused on environmental and climate change on TP (Xu et al., 2009; Yang et al., 2011; Yao et al., 2012), particularly in the Himalayan region (Lau et al., 2006; Gautam et al., 2009). Although TP has pristine atmospheric conditions with quite low aerosol load in annual average (Cong et al., 2009), both anthropogenic

ACPD
13, 20961–21002, 2013

and natural aerosols can be transported there (Cong et al., 2007). Some extreme contaminative events in the central TP indicate that pollutions extending to 3–5 km above sea level (a.s.l.) could be transported to TP by the southwesterly prevailing winds (Xia et al., 2011). Dust also influences TP greatly, and Tibetan airborne dusts appear to be largely associated with surrounding source regions, for example, Taklimakan desert (Xia et al., 2008), Tarim Basin, Gobi Desert, northwest India and Middle East (Huang et al., 2007; Liu et al., 2008). The concentration of aerosols decreases rapidly with increasing altitude over the Himalayan region, and Ångström exponent (AE) remains high in the well mixed region but decreases above (Dumka et al., 2011). Black carbon (BC) transported to the Himalayas and the Tibetan Plateau (HTP) has increased in recent years, and South Asia and East Asia are the two main source regions (Lu et al., 2012). Large abundance of BC in central Himalayas is related to the boundary layer dynamics and the human activities in the adjoining valley (Pant et al., 2006). The Himalayas blocks BC particles across the mountains into the plateau, but Yarlung Tsangpo River valley acts as a "leaking wall" to contaminate the southeast TP (Cao et al., 2011).

Both seasonal and diurnal variations of aerosols are important to investigate aerosol optical properties. The characteristic time scale of variation of AOD is about 3 h in remote regions, but can be less than 1 h near the emission sources (Anderson et al., 2003). The characteristics of total aerosol or carbonaceous aerosol daytime variations have been studied at many regions, such as North and South America (Zhang et al., 2012), South Asia (Singh et al., 2004; Pandithurai et al., 2007; Gautam et al., 2011), China (Wang et al., 2004).

Remote sensing retrieval of AOD has been applied in many regions (Li et al., 2007; He et al., 2010; Breon et al., 2011), but with much uncertainty on the TP for its low aerosol load (Wang et al., 2007). This paper analyzes the seasonal characteristics of fine and coarse mode aerosols respectively using AERONET data. Diurnal variations of aerosol optical properties are revealed and potential causes are also discussed. The data and methodology are described in Sect. 2. The spatial feature of precipitation and wind field are presented as meteorological feature in Sect. 3.1. The seasonal aerosol

ACPD
13, 20961–21002, 2013

optical properties are analyzed in Sect. 3.2, and the diurnal aerosol variations are discussed in Sect. 3.3. Conclusions are given in the Sect. 4.

2 Datasets and methodology

2.1 Site descriptions

Three AERONET sites (QOMS_CAS, EVK2-CNR and Pokhara) are selected for this study. QOMS_CAS is on the northern slope of Himalayas, and the other two sites are on the southern slope. The climatic conditions are different between the southern and northern slopes. The information of these three stations is listed in Table 1. The date ranges show the investigated period used to calculate annual means, seasonal values and diurnal variations. The topography and the observation environment are shown in Fig. 1.

QOMS_CAS (China, Table 1, Fig. 1) is located at a northeast-southwest valley in the Everest region. In monsoon season, the leading surface wind direction is southwest, while in other seasons the dominant surface wind direction is northeast. Southwesterly winds prevail during the monsoon season, and in other period the westerly winds prevail (Ma et al., 2011; Li et al., 2012). EVK2-CNR (Nepal, Table 1, Fig. 1) is located at the foothill of Mount Everest in a north–south valley. The surrounding areas are dominated by large moraines and high mountains (5800–6200 m a.s.l.). The wind regime is characterized by an evident mountain-valley circulation. The leading surface wind direction is south during daytime all year long. Only during the non-monsoon season, the mountain winds prevail during nighttime and northwesterly winds are observed due to the influence of the westerly winds (Bonasoni et al., 2008; Bonasoni et al., 2010; Gobbi et al., 2010). Pokhara (Nepal, Table 1, Fig. 1), an urban site in Nepal, is situated in the northwestern corner of the Pokhara Valley. As a result of sharp rise in altitude, Pokhara has one of the highest precipitation rates in its country. Summer is humid and

ACPD
13, 20961–21002, 2013

mild, and most rainfall occurs during the monsoon season (July–September). Winter and spring skies are generally clear and sunny (Kansakar et al., 2004).

2.2 AERONET data

AERONET is a federated international ground-based global network established for characterizing aerosol optical properties and validating aerosol satellite retrievals. This network has more than 800 stations globally, using the unified data correction methods to ensure the quality of data (Holben et al., 1998). Derived from the AERONET network, ocean, desert dust, biomass burning and urban aerosol physical properties have been studied by previous researches (Dubovik et al., 2002a; Smirnov et al., 2002b). CIMEL sunphotometers deployed by AERONET can measure aerosol optical properties using two observation modes. First, CIMEL radiometers make measurements of the direct sun radiance at eight spectral channels (340 nm, 380 nm, 440 nm, 500 nm, 675 nm, 870 nm, 940 nm, and 1020 nm) to acquire the aerosol optical depth, and use spectral channels of 940 nm to get water vapor content. Then, CIMEL could also make sky diffuse radiation measurements at four spectral channels (440 nm, 675 nm, 870 nm and 1020 nm) to acquire aerosol microphysical and optical properties (Holben et al., 1998, 2001). Parameters such as aerosol size distribution, single-scattering albedos, asymmetry factor and refractive index are obtained by the inversion algorithm (Dubovik and King, 2000; Dubovik et al., 2002b). The uncertainty in AOD for Level 2 AERONET data is 0.01 to 0.02 (Eck et al., 1999). The less aerosols are in the atmosphere, then the larger uncertainty comes (Dubovik and King, 2000). The wavelength (λ) dependence of AOD is characterized by AE with a classical empirical equation $\mathrm{AOD}(\lambda) = \beta\lambda^{-\mathrm{AE}}$ (β means turbidity coefficient) (Ångström, 1929, 1964). The uncertainties in computed AE are much larger at low AOD (Kaskaoutis and Kambezidis, 2008; Kreuter et al., 2013). However, the quantitative uncertainty in AE for AERONET data is lacking. In addition, contamination by undetected clouds and hygroscopic growth of aerosol particles leads to a decrease of AE and an increase of AOD in the humid environment surrounding clouds (Chand et al., 2012). However, the effects of clouds are ignored in this study. At

ACPD
13, 20961–21002, 2013

present, AERONET has level 1.0, level 1.5 and level 2.0 data product, which denotes raw data, automatically cloud cleared data and manual inspected data. In this study, we mainly use level 2.0 data, and have an alternative in level 1.5 data for the case of missing level 2.0 data.

2.3 Satellite data and reanalysis data

In this study, level 3 TRMM precipitation products (3B43 version 7 and 3B42 version 7), are used to show spatial rainfall feature and rainfall daytime variations. Temporal resolution of 3B43 data is a month, and its spatial resolution is 0.25° × 0.25°. The temporal resolution of 3B42 data is 3 h, and the spatial resolution is same as 3B43 (Huffman et al., 2007). Because the winter of 2012 is defined from December 2012 to February 2013 in this study, TRMM 3B43 data in 2013 are not available at present. Although 2010 to 2012 are the same observation periods among three sites, we only use the data of 2010 and 2011 to get spatial feature. To get the monthly precipitation, we simply do the conversion by multiplying the hourly rain rate with the total hours in that month using 3B43 product. We can get the total amount of precipitation in a season by adding up the monthly precipitation in that season. To reflect the actual rainfall during the observation periods, we average the accumulated precipitation of 2010 and 2011 in each season. The following subsections would elaborate on the classifications of seasons. 3B42 data are used to get rainfall daytime variations. TRMM data are used to analyze diurnal rainfall changes rather than station observations. Compared with station data, TRMM data have same observation mode, same data processing and better continuity at these three stations. We extract the values from the grids which these stations are located at to get time series of precipitation. Using the extracted values at different time, we can obtain the diurnal variations of precipitation rate (PR) in all seasons. For diurnal variations, the date ranges of TRMM 3B42 data are selected in accord with AERONET data at each station.

NCEP/NCAR reanalysis monthly means are used to show the wind field at 850 hPa. The temporal resolution of reanalysis data is a month, and its spatial resolution is

ACPD
13, 20961–21002, 2013

2.5° × 2.5°. The date ranges of wind field data are selected in accord with TRMM data. The seasonal means of wind field are calculated by averaging the monthly means in each season. NECP/NCAR reanalysis data (2.5° × 2.5°, 6 h temporal resolution) are also used for back-trajectory calculations. The five-day air mass backward trajectories are calculated by Hybrid Single-Particle Lagrangian Integrated Trajectory (HYSPLIT) model version 4.9. Back trajectories are run every six hours for April and July in 2012. The arrival height is set as 1 km above ground level (a.g.l.).

2.4 Analysis methods

Total AOD at 500 nm, fine mode AOD at 500 nm and AE at 440–870 nm are selected to exhibit the aerosol optical properties throughout the year. Total AOD reflects the extinction of both coarse and fine mode aerosols, and fine mode AOD only reflects the extinction of fine mode aerosols. Some unrealistic measurements need to be eliminated. The data that fall within 0.01 < total AOD < 3, 0 < fine mode AOD < 3 and 0 < AE < 3 at the same time are only considered. Box and whisker plot is used to analyze the aerosol properties. The median is better to represent the seasonal characteristics than the mean, because the mean is greatly influenced by some extreme events. If the median is lower than the mean, the parameters of aerosols have high values in extreme events, and vice versa. Fine mode fraction (FMF) at 500 nm defined as the ratio of fine mode AOD to total AOD is a quantitative parameter. In this study, FMF is calculated by dividing the seasonal median of total AOD by fine mode AOD in each month. FMF can be used to analyze the seasonal variations of particle size and deduce the major aerosol type (He et al., 2012a). Single scattering albedo (SSA) is usually used to judge the aerosol type as well. Some studies have successfully combined SSA with other parameters to determine the aerosol type over different regions (Lee et al., 2010; He et al., 2012b; Logan et al., 2013). However, the region with low aerosol load (AOD 440 nm < 0.44) is difficult to obtain aerosol type by SSA with adequate accuracy (Dubovik and King, 2000). Another graphical method to classify aerosols needs

ACPD
13, 20961–21002, 2013

AOD > 0.15 with enough accuracy (Gobbi et al., 2007). Therefore, these methods are not suitable in this study.

The instantaneous data of AOD and AE are used to get diurnal variations. This AOD is roughly equal to total AOD. But AOD data have a much longer time series because calculating total AOD and fine mode AOD needs some hypothesises. Thus the diurnal variations of total AOD and fine mode AOD are not calculated due to their rare data and poor continuity. The reason for using AE instead of FMF to evaluate the daytime variations of aerosol size is for the same reason. However, some unrealistic measurements need to be eliminated too. We also choose the normal range of values, which are in the ranges of $0.01 < AOD < 3$ and $0 < AE < 3$. All the observations in a day are expressed as a departure percentage from the daily mean (Smirnov et al., 2002a). In this study, we don't use the division of monsoon season and non-monsoon season to analyze diurnal variations of AOD and AE. Because there is no unified classification standards for monsoon season over this region. In addition, South Asia monsoon influences the study region at different periods in each year. Though these three stations are close, the onset and decay dates of South Asia monsoon are not the same in the study years. So we divide the data into four usual seasons, namely, March to May (MAM), June to August (JJA), September to November (SON) and December to February in the next year (DJF). This division method makes a better comparison with other studies in other regions. In each period, we compute the hourly mean of AOD and AE, for example, between 10:00 and 11:00 local time (LT) in each day. And we need to change UTC time to LT in the data files. If the available hourly means in a day are less than five hours, the day would be excluded. Then the percentage and absolute departures of each hourly average are calculated from the daily mean. The diurnal variations in each season are calculated by aggregating all hourly departures of different local hours in one season. If all available days in a season of a particular year are less than ten, this season would be excluded. That is because the observation days are too rare to represent the daytime variation pattern in one season. We can get the multiyear diurnal

ACPD
13, 20961–21002, 2013

variation by averaging that in each year. Diurnal variations of PR are calculated by the same method using TRMM data.

3 Results

3.1 Meteorological feature

Regional meteorology is one of the key factors that influence aerosol optical properties. Figure 2 shows the seasonal variations of precipitation and prevailing winds at 850 hPa. Precipitation is the highest in summer, followed by in spring, and the lowest in winter. In MAM, South Asia monsoon begins to develop and southwest winds blow towards the southeast TP. Precipitation is less than 100 mm in the whole TP during this period. The southeast TP is a bit wetter than other regions. In JJA, southwest or south winds prevail in the Himalayan region and northern India. Rainfall increases significantly, for winds bring much moisture. Precipitation is more in the southern part of TP than the northern part. The Himalayas plays an important role in blocking moisture to the main body of TP. In most of the southern slope of Himalaya, precipitation is more than 1200 mm. Rainfall decreases significantly in SON with the retreat of monsoon. South winds prevail only in the northeast of India in autumn. During winter, the regional dominant wind direction is northwest, and precipitation is less than 100 mm in most regions of TP.

In short, mechanical forcing and unique elevated thermal forcing have a large impact on regional as well as global climate. The mechanical and thermal forcing by TP makes the relative contributions of the climbing and deflecting effects of mountains (Wu et al., 2012). This mechanism greatly influences the transport of air particles and moisture (Wu et al., 2007; Cao et al., 2011). The Himalayas acting as a natural barrier is essentially attributed to the mechanical and thermal forcing effects of TP. Therefore, the southern slope of Himalayas and northern India has much more precipitation than TP, especially in summer and autumn.

ACPD
13, 20961–21002, 2013

3.2 Seasonal variations

The annual mean of AOD during the investigated period was 0.06 at QOMS_CAS, 0.04 at EVK2-CNR and 0.51 at Pokhara respectively. Pokhara is an urban site with much higher aerosol load according to the annual means. Monthly statistics of aerosol properties are presented in Figs. 3–5. And different stations have different seasonal characteristics.

Total AOD (Fig. 3) is quite low at QOMS_CAS and EVK2-CNR, but much higher at Pokhara. Because urban/industrial and fuel combustion emissions do have a significant impact on the atmospheric environment at Pokhara (Sharma et al., 2012). At QOMS_CAS, the maximum seasonal mean of 0.12 occurs in July. However, the maximum seasonal median of 0.09 occurs in May. All monthly means are higher than monthly medians, indicating the contributions of some events with higher aerosol load. Both seasonal mean and median are less than 0.10 except July, suggesting pristine atmospheric conditions during these months at QOMS_CAS. In addition, the lower aerosol load is recorded from September to December. Total AOD at EVK2-CNR shows a similar variation pattern to that at QOMS_CAS. And all monthly means are higher than monthly medians as well. The maximum seasonal mean and median both occur in August, and they are 0.17 and 0.09 respectively. The mean in August at EVK2-CNR is about two times higher than that at QOMS_CAS, while the median in August at EVK2-CNR is 1.5 times as high as QOMS_CAS. This phenomenon illustrates the Himalayas blocks the aerosol particles across the mountains during the monsoon season. Both seasonal mean and median are less than 0.04 from November to January at EVK2-CNR. Unlike QOMS_CAS and EVK2-CNR, total AOD shows two peak values at Pokhara. The seasonal mean and median have similar seasonal patterns, but the peak months are different. The peak values of seasonal means occur in April and November, while the peak values of seasonal medians are in April and October. All monthly means are higher than monthly medians, especially in November. The aerosol load is lower

ACPD
13, 20961–21002, 2013

from July to September than other months, resulting from the large rainfall during the monsoon season.

The seasonal variations of fine mode AOD (Fig. 3) are different from total AOD at QOMS_CAS and EVK2-CNR. The maximum seasonal mean and median are both in April. The higher fine mode AOD is recorded in April at both QOMS_CAS and EVK2-CNR. Previous studies revealed that March to June was major fire season in the low altitude areas in the Himalayan region (Vadrevu et al., 2012). Smoke aerosols released from strong forest fires in northern India and Himalayas can be transported above the planetary boundary layer by deep convection (Vadrevu et al., 2008; Tosca et al., 2011), which can be further transported to central TP by atmospheric circulations (Xia et al., 2011). At EVK2-CNR, the maximum seasonal mean and median are both in April too. The higher aerosol load is recorded during March to June and August. Fine mode AOD from March to June is lower at EVK2-CNR than at QOMS_CAS, but is higher in August. This indicates the Himalayas blocking fine mode aerosols mainly occurs during the monsoon season. On the contrary, the seasonal distribution of fine mode AOD is similar to total AOD at Pokhara. The maximum seasonal mean and median occur in April, and the lower seasonal values are recorded from July to September. The monthly mean of fine mode AOD is about two times higher than median in November, due to some extremely high aerosol load events. For instance, total AOD is 2.50 and fine mode AOD is 2.46 at 3 November 2011. These extreme events may be influenced by agriculture crop residue burning over the Indo-Gangetic Basin during November (Mishra and Shibata, 2012).

The HYSPIT analysis is used to show the impact of long-range transportation of smoke and dust aerosols more clearly. April and July in 2012 are selected as examples to shown the potential aerosol sources (Fig. 6). Due to relatively close locations and similar aerosol sources, the frequency plots of 5 day back trajectories at QOMS_CAS are shown (the plots at the other stations are not shown). Based on the frequency plot of 5 day back trajectories at 1 km a.g.l. in April, most of the air masses come from the west, agreeing well with the prevailing westerly winds. And the Himalayas and north-

ACPD
13, 20961–21002, 2013

ern India are the major source regions. Therefore, vegetation fires in the Himalayan region and northern India influence the environment in Everest region significantly during this period, as well as the other two sites. The frequency plot in July indicates that South Asia monsoon may carry aerosols to the study sites. Airflows mainly come from two directions which are in accord with two branches of South Asia monsoon. The airflow originating from Arabian Sea may transport dust from northwest India (e.g. Thar Desert) to the study sites. Thus dust may have a significant impact on these stations. This is similar to the results of previous studies (Carrico et al., 2003). The above results provide the potential aerosol sources. But the results are not absolutely accurate due to the uncertainty and disadvantage of HYSPLIT model (Koracin et al., 2011).

AE (Fig. 4) shows two peak values at QOMS_CAS. The seasonal mean and median in April and December (> 1.0) are higher than other months. The seasonal means are lower from July to September, while the seasonal medians are lower in July and August. It suggests that fine particles may account for the majority of the aerosol volume concentration in April and December, but the minority during monsoon season. The seasonal pattern of AE at EVK2-CNR is similar to that at QOMS_CAS from April to December. The maximum seasonal mean and median AE (> 1.0) occur in January. AE is a little higher in April and winter, while lower in July and August. At Pokhara, the highest value of AE occurs in September, and the lowest value occurs in July. The seasonal mean and median, more than 1.0 except July, are much higher than the other two stations. Seasonal mean and median of AE from September to February (> 1.3) indicate the majority of the aerosol volume concentration consisted of fine particles during these months. AE is a bit higher in April, resulting from fire emissions in the Himalayas.

FMF (Fig. 5) can also reflect the particle size, and FMF nearly changes in accord with AE at each site. But there are still some differences between AE and FMF. Because AE can be changed according to the effective radius of the fine mode aerosol and the ratio of fine mode to total volume concentration (Lee et al., 2010). At QOMS_CAS, the maximum FMF of 0.78 occurs in April. FMF is much higher in April and May than other months (< 0.60). The relative lower FMF is recorded from June to August, and the

ACPD
13, 20961–21002, 2013

minimum FMF of 0.37 occurs in August. This indicates that the aerosol compositions are dominated by fine particles in April and May at QOMS_CAS. Coarse particles account for the majority of the aerosol volume concentration in August. At EVK2-CNR, the lower values of FMF occur from July to September. FMF is less than 0.40 during these months, which is apparently lower than that at QOMS_CAS. It suggests that the majority of the aerosol volume concentration consisted of coarse particles at EVK2-CNR, which may be associated with the dust transported to the station during these months. FMF is a little more than 0.60 in February and November. At Pokhara, FMF is more than 0.60 except July. Therefore, fine mode particles account for the majority of the aerosol volume concentration at Pokhara.

Monthly precipitation (Fig. 5) is analyzed at these sites. The three sites show similar seasonal pattern of precipitation. The maximum precipitation occurs in July at all sites. The average precipitation in July is 200 mm at QOMS_CAS, 301 mm at EVK2-CNR and 519 mm at Pokhara, respectively. From April to September, the monthly precipitation is highest at Pokhara, and followed by at EVK2-CNR. Conversely, precipitation at Pokhara is lower than the other two sites from October to March. The monthly precipitation is less than 60 mm at the three sites during these months. The inter-annual difference of precipitation is usually higher from April to September than other months at the three sites.

In summary, QOMS_CAS and EVK2-CNR do have a pristine environment. However, Pokhara is seriously affected by human activities. Both total AOD and fine mode AOD at Pokhara are much higher than other two sites in each season. Vegetation fires peak in the Himalaya region in April (Vadrevu et al., 2012), which makes an enormous impact on all the three sites. Dust can be also transported to these sites during the monsoon season.

ACPD
13, 20961–21002, 2013

3.3 Diurnal variations

3.3.1 Precipitation rate

To interpret the possible effects of rains, the diurnal cycle of PR is analyzed (Fig. 7). The diurnal variations of precipitation show a consistent pattern in each season among years, such as obvious higher PR (not shown). And only diurnal variations of the average PR are displayed. The daytime variation range is the largest in summer at all the sites, and the smallest in winter. The inter-annual fluctuation is larger in summer. PR at Pokhara is higher than at the other two high-altitude stations, and PR at EVK2-CNR is a bit higher than QOMS_CAS. The PR peak at each site generally occurring in the late afternoon may be related to the strong interaction between meso-scale convective systems and steep terrain (Barros et al., 2000).

The diurnal variations of PR do not show similar patterns in each season at QOMS_CAS. PR is less than 0.1 mm h^{-1} during the day in MAM. Rainfall mainly occurs in the afternoon in JJA. The lowest PR in summer is close to zero at 09:00 (LT, the time below is LT without a specific instruction). PR rises sharply from 12:00 to 15:00, and then fluctuates within a narrow range until midnight. The peak value of PR is observed in SON and DJF but the occurrence time is different.

PR is higher at EVK2-CNR than at QOMS_CAS except in winter. PR in spring (MAM) and autumn (SON) is about 0.2 mm h^{-1}, but in winter (DJF) is less than 0.1 mm h^{-1}. No evident peaks or obvious patterns are found in MAM, SON and DJF. It rains more from the afternoon to midnight rather than in the morning in MAM. However, there are no similar consequences in SON and DJF. In JJA, PR decreases from 3:00 to 6:00, then increases slowly from 6:00 to 15:00. PR increases dramatically from 15:00 to 18:00, reaches the maximum at 18:00, and then decreases sharply.

Daytime variations of PR in each season at Pokhara are clearly different from the other two stations with high altitude. It has the highest precipitation among these three stations. In MAM, a higher PR value (about 0.46 mm h^{-1}) occurs at 18:00. No significant rainfall occurs in the rest of the day. In JJA, rainfall decreases before 15:00 and then

ACPD
13, 20961–21002, 2013

increases. Lower PR (about 0.18 mm h^{-1}) occurs at noon and early afternoon (12:00 to 15:00). That means more rainfall occurs in the late afternoon and night. The diurnal variations of PR in SON look like JJA to some extent. However, PR is much lower in SON than in JJA. There is no significant rainfall in winter.

3.3.2 AOD at 500 nm

The diurnal variations of AOD at 500 nm are shown in Fig. 8. Different stations have different diurnal variation patterns. At QOMS_CAS, the diurnal variations of AOD do not have similar patterns among seasons, and the relative daytime variation range is less than 20 % except in summer. At EVK2-CNR, AOD almost increases from morning to sunset in all seasons, and the relative daytime variation ranges are larger than at the other two sites. At Pokhara, AOD decreases from early morning, reaches to minimum at noon, and then increases significantly except in summer. The relative daytime variation range at Pokhara is a bit larger than at QOMS_CAS. However, the absolute daytime variation range of AOD at Pokhara is the largest. The absolute daytime variation range of AOD is quite small at QOMS_CAS and EVK2-CNR, and can be comparable to the uncertainty of AERONET AOD measurements in some seasons. The consistent daytime variation pattern by multi-year observations may indicate the physical processes.

At QOMS_CAS, the diurnal variations of AOD do not have similar patterns among seasons. The diurnal cycles have great differences among multiyear observations in spring, autumn and winter (not shown). In spring (MAM), the daytime variation range of AOD is generally small. In summer (JJA), AOD changes little from morning to 15:00, and then decreases sharply in the late afternoon. This sharp decrease can be associated with rainfall at later afternoon, deduced from TRMM data. In autumn (SON) and winter (DJF), the daytime variation range is less than 20 %. Generally the relative daytime variations in spring are smallest, and in summer are largest. Correspondingly, the absolute daytime variation range of AOD is about 0.03 in summer, and it is usually below 0.02 in other seasons.

ACPD
13, 20961–21002, 2013

At EVK2-CNR, the diurnal variations of AOD show similar patterns in all seasons with different magnitude. AOD has small fluctuations from 7:00 to 10:00, and then increases in spring, summer and autumn. AOD increases from morning to sunset in winter. The relative daytime variation range is about 103 % in MAM, 57 % in JJA, 54 % in SON and 66 % in DJF, respectively. Correspondingly, the absolute daytime variation range of AOD is about 0.06 in MAM, 0.05 in JJA, 0.02 in SON and 0.02 in DJF. The absolute daytime change is related to monthly average AOD. Lower relative daytime variation but larger absolute daytime variation occurs in summer, which may be due to higher aerosol load during monsoon season. Because of lacking effective observations in the late afternoon, whether large rainfall would remove aerosols cannot be known in summer.

At Pokhara, the diurnal cycles of AOD in all seasons are similar and repeatable between different years (not shown). The diurnal variations of AOD show a similar pattern in spring, autumn and winter. In these three seasons, AOD decreases from early morning, reaches to minimum at noon, and then increases significantly. Peak values of AOD are reached at 8:00 in the morning and at 17:00 in the late afternoon, which may be consistent with BC emissions from biofuel cooking at a fixed time (Rehman et al., 2011). In MAM, AOD at 18:00 drops quickly, which is due to wet deposition of precipitation. This phenomenon does not happen in autumn and winter, because rainfall does not have an evident peak during the day. As a result of large rainfall, the diurnal variations are different in summer. The relative daytime variation range in summer is about 10 %, and much smaller than other seasons. Correspondingly, the absolute daytime variation range of AOD is about 0.20 in MAM, 0.04 in JJA, 0.10 in SON and 0.08 in DJF.

3.3.3 AE at 440–870 nm

The diurnal variations of AE at 440–870 nm are shown in Fig. 9. At QOMS_CAS, AE decreases first in the morning and then increases in the afternoon in each season. And the relative daytime variation range is the largest at QOMS_CAS. The diurnal cycle at

ACPD
13, 20961–21002, 2013

EVK2-CNR is similar to that at QOMS_CAS except in summer. No significant diurnal variations of AE are found at Pokhara. The relative daytime variation range at Pokhara is the smallest. However, the larger relative daytime variation range can be partly due to greater AOD uncertainties at QOMS_CAS and EVK2-CNR. The uncertainty of AE is larger at low aerosol load.

At QOMS_CAS, the diurnal variations of AE have similar patterns in all seasons. AE drops from the morning, reaches to minimum at noon or the early afternoon and then reverses to increase. The patterns of diurnal curves are similar between multiyear observations but with different magnitude and phase (not shown). The relative daytime variation range is about 36 % in MAM, 63 % in JJA, 79 % in SON and 45 % in DJF. Correspondingly the absolute daytime variation range is 0.35, 0.32, 0.54 and 0.36, respectively. AE is a qualitative indicator, and it can only show the relative particle size. The above results indicate smaller particles in the morning and late afternoon, and relatively larger particles at noon in all seasons.

The diurnal cycle at EVK2-CNR is similar to that at QOMS_CAS. However, the diurnal variations have great inter-annual differences with different magnitude and phase in spring and autumn (not shown). In summer, AE increases from 7:00 to 10:00, decreases a little from 10:00 to 14:00, and then increases again. This phenomenon results from uneven precipitation at EVK2-CNR. In winter, the daytime variation pattern is quite similar to that at QOMS_CAS. The relative daytime variation range is 35 % in MAM, 26 % in JJA, 23 % in SON and 32 % in DJF. And the relative ranges are very close among all seasons. Correspondingly, the absolute daytime variation range is 0.32, 0.18, 0.26 and 0.37, respectively.

At Pokhara, AE changes little during daytime in MAM, SON and DJF. Specifically, the relative daytime variation range is less than 6 % in spring, autumn and winter, but about 20 % in summer. The absolute daytime variation range of AE is less than 0.12 in spring, autumn and winter, but about 0.25 in summer. This result indicates the average aerosol particle size hardly change in MAM, SON and DJF. However, AE increases significantly in the late afternoon in JJA. TRMM results indicate that rainfall begins to

ACPD
13, 20961–21002, 2013

increase from 15:00 to 18:00. Therefore, large rainfall in summer plays an important role in wet deposition, and more coarse mode aerosols than fine mode are deposited by precipitation scavenging effect.

3.3.4 Possible factors contributing to aerosol daytime variations

The diurnal variations of AOD and AE are due to many factors, such as rainfall, emissions, mountain-valley circulations, surface heating and so on. The major factors are discussed in sections below.

Uneven diurnal precipitation leads to the great change of aerosol properties by precipitation scavenging effect. The precipitation is effective in removing the aerosols, which can result in a decrease of the average aerosol size in a fixed time. For example, the diurnal peak value of rainfall exists in spring at Pokhara. AOD decreases, but AE increases slightly. The same phenomenon happens in autumn at QOMS_CAS. In addition, more rainfall happens in the afternoon or the late afternoon in summer at all the three stations. Wet deposition changes the aerosol load and the average particle size.

Aerosol properties are also impacted by the diurnal emission rate. It is certainly related with the distance between the station and the emission source. The sun photometer is located in Pokhara city, highly influenced by emission source. Previous studies found that the diurnal mean concentration of PM_{10} was higher in the morning (7:30 a.m. to 11:30 a.m.) and evening (3:30 p.m. to 7:30 p.m.) than afternoon (11:30 a.m. to 3:30 p.m.) at Pokhara (Bashyal et al., 2010). The PM_{10} represents the emission characteristics in the city to a certain extent. So the higher AOD is observed in the morning and the early evening during the day. Man-made pollutions mainly consist of fine particles, so AE changes very little during the day. Thus, the diurnal variations of aerosols may be related with the emissions from human activities. Conversely, the above phenomenon does not take place at QOMS_CAS and EVK2-CNR, because these two sites are both located at high altitude areas and far away from anthropogenic emission sources.

ACPD
13, 20961–21002, 2013

Mountain-valley circulations also influence the transport and removal of aerosols on a daily time scale. EVK2-CNR is greatly influenced by valley wind during daytime. The airflow of valley wind continues to carry aerosols from lower polluted region, which leads to the ever-increasing AOD. The other two stations are not located in the mountain without the valley winds, so the phenomenon does not appear.

Moreover, surface heating has an enormous impact on the local convections, which greatly influence the aerosol vertical exchange between ABL and free troposphere and the diffusion rate of pollutions. As the sun rises, surface heating enhances gradually, reaches to maximum at about 12:00, and then weakens again (Ma et al., 2005). The convections change in accord with surface heating (Yanai and Li, 1994). The parameters of aerosols reflect the properties of the whole atmosphere. If aerosols just exchange between upper and lower atmosphere, the vertical distribution of aerosols would change. But the aerosol properties are nearly invariable. If the flow of aerosols into or out of the observation region has changed, the aerosol properties would change accordingly. At QOMS_CAS, AOD does not show a consistent daytime variation pattern, while AE has a similar pattern in each season. What are the reasons of this interesting phenomenon? Local aerosols, dominating in the lower atmosphere, are predominantly composed of natural emissions at Everest region. Surface wind speed is crucial for picking up coarse mode aerosols from the earth surface to the atmosphere (Kok, 2011). The surface wind speed always increases greatly in the afternoon (Sun et al., 2007). The aerosols in upper atmosphere like free troposphere (FL) mainly consist of long-range transport aerosols. Aerosols in the lower atmosphere may have a clear daytime variation pattern related to wind speed. Conversely, long-range transport aerosols are of great randomness on a diurnal time scale. The changes at lower and upper atmosphere are combined together, which lead to different diurnal variations of AOD among seasons or multiyear observations. And different size aerosols blended contributes to the similar diurnal variations of AE. The aerosol particle size in upper atmosphere like free troposphere (FL) is much smaller than aerosols in surface layer (SL). Surface heating enhances gradually in the forenoon, which make convec-

ACPD
13, 20961–21002, 2013

tions strengthen. The more intensive the convection is, the more large particles can be transported into the troposphere. And the particle size in the upper atmosphere is small and changes little. Therefore, the concentrations of large particles continually grow and the column-integrated particle size becomes larger in the forenoon. Instead, convection weakens in accord with the change of surface heating in the afternoon. Accordingly, the aerosol particle size becomes smaller gradually from noon to late afternoon. The aerosol load in upper atmosphere is comparable to that in the lower atmosphere. The aerosol properties are sensitive to the whole atmosphere. In other words, no matter the aerosols in upper or lower atmosphere vary, AOD or AE would change accordingly at QOMS_CAS during daytime. The environment at EVK2-CNR is similar to QOMS_CAS, and the similar convection process happens. So the diurnal variations of AE in autumn and winter are similar to QOMS_CAS. Nevertheless, the diurnal variations of AE have another pattern and show great differences among multi-year measurements in spring at EVK2-CNR. The Himalayas blocks most of the coarse particles across the mountains. Fine and coarse mode particles are mixed to make atmospheric composition more complex on the southern slope, which result in the great inter-annual difference of diurnal curves in spring. The surface heating and convections happen at Pokhara too. Convections make the pollution transport upward so that the pollution concentration would drop at the surface. Nevertheless, the pollution in the upper atmosphere would increase. The airflow in or out of the observation region can change aerosol properties greatly, regardless of the vertical distribution. Convection becomes stronger and stronger in the forenoon, and the diffusion of pollutants into the surrounding region enhances gradually. Thus, AOD decreases in the forenoon. Conversely, convection as well as pollutant diffusion rate weakens gradually in the afternoon. Thus, AOD increases in the afternoon during daytime.

ACPD
13, 20961–21002, 2013

4 Conclusions

We have investigated seasonal and diurnal aerosol optical properties from three AERONET sites around the Himalayan region. The critical factors are different at the two time scales. As expected, seasonal changes are profoundly affected by large scale atmospheric circulation. Diurnal variations are mainly influenced by meso-scale systems and local topography.

Aerosols optical properties exhibit seasonal change patterns in the Himalayas. While observations at QOMS_CAS and EVK2-CNR can generally be representative of a remote background atmosphere, Pokhara is an urban site polluted by human activities. Vegetation fires in the Himalayan region and northern India can release large amount of smoke aerosols especially in April (Andreae and Merlet, 2001), leading to a growing fine mode aerosol load at QOMS_CAS and EVK2-CNR. Although there is large rainfall in summer, the effect of southwest winds carrying dust is stronger than wet deposition at QOMS_CAS and EVK2-CNR. The dust concentration may build up in between the rainy days. Coarse mode AOD at EVK2-CNR is higher than QOMS_CAS from July to September, indicating the Himalayas plays a significant role in blocking the coarse particles brought by the southwest winds. The atmosphere environment has been seriously polluted by human activities at Pokhara, leading to much higher aerosol load than the other two stations. The seasonal peak values of total AOD and fine mode AOD are observed in April and November, and lower aerosol load occurs in July and August. The first peak occurs in April at Pokhara for the same reason as the other two sites, and the second peak in November is associated with crop residue burning. Conversely, large rainfall can remove aerosols effectively, which contributes to lower aerosol load in July and August.

These stations show different daytime variation patterns, depending on season. Similar diurnal variation patterns of AOD are not observed in each season at QOMS_CAS, but are found at the other two stations. AOD nearly increases from morning to sunset in all seasons at EVK2-CNR. And AOD decreases from early morning, reaches

ACPD
13, 20961–21002, 2013

to minimum at noon and then increases significantly except in summer at Pokhara. The relative daytime variation range of AOD at EVK2-CNR is the largest, and is a bit larger at Pokhara than at QOMS_CAS. The absolute daytime variation range of AOD at Pokhara is the largest, and quite small at QOMS_CAS and EVK2-CNR. Because the absolute daytime variation range of AOD is closely related to the aerosol load at each station. At QOMS_CAS, AE decreases first in the morning and then increases in the afternoon in each season. And the daytime variation pattern in autumn and winter at EVK2-CNR is similar to that at QOMS_CAS. But the diurnal cycle of AE is not significant at Pokhara. The relative daytime variation range of AE is the largest at QOMS_CAS, and the smallest at Pokhara.

The diurnal variations of AOD and AE are affected by many factors, such as rainfall, emission sources, mountain-valley circulations, surface heating and their interactions. Uneven diurnal precipitation leads to the great change of aerosol properties by precipitation scavenging effect. Precipitation can reduce the aerosol load and result in a decrease of the average particle size. Aerosol properties are also impacted by the characteristics of diurnal emissions and the distance from the emission source. Pokhara is near the emission source, and the enhanced emissions can result in an increase of AOD in the morning and late afternoon. The other two stations are far away from the emission source so the aerosol load would not change immediately with the emissions. Mountain-valley circulations also influence daytime aerosol variations. Because valley winds prevail during daytime in each season at EVK2-CNR, AOD continuously increases. The surface heating has an enormous impact on the local convections, and the convections influence the vertical aerosol exchange as well as the diffusion rate of pollutions. The aerosol parameters reflect the aerosol change in the whole atmosphere. The aerosol exchange between the upper and lower atmosphere can change the vertical distributions of aerosols, but has no significant influence on aerosol properties. The aerosol properties would change accordingly with the flow of aerosols into or out of the observation region. At QOMS_CAS, aerosols in the lower atmosphere may have a clear daytime variation pattern. Nevertheless, long-range transport aerosols in

ACPD
13, 20961–21002, 2013

the upper atmosphere are of great randomness on a daily time scale. Therefore, AOD does not have a consistent diurnal variation pattern at QOMS_CAS. The diurnal variations of convections have its inherent laws due to surface heating. Large particles are picked up from the surface into the atmosphere by strong convection. However, the particle size in the upper atmosphere is small and changes little. Thus, the aerosol particle size changes in accord with the convection during daytime at QOMS_CAS. The diurnal variations of AE in autumn and winter at EVK2-CNR are similar to QOMS_CAS, because the similar convection process happens. However, there is greater inter-annual difference in diurnal curves of AE in spring at EVK2-CNR. The surface heating and convections make the pollution transport upward so that the pollution concentration would drop at the surface at Pokhara. Nevertheless, the pollution in the upper atmosphere would increase. The strength of convection controls the vertical exchange and the diffusion rate of pollutions. AOD decreases in the morning with an enhanced convection, but increases in the afternoon with a weakened convection at Pokhara.

Although we confirm that aerosols come from long-range transport and vicinity region, we can only discuss aerosol source qualitatively. We cannot give the exact proportions, no matter on seasonal time scales or diurnal time scales. It is deduced that the aerosol load in lower atmosphere is comparable to that in the upper atmosphere at QOMS_CAS on a daily time scale. And the aerosol load in lower atmosphere is a bit more than that in the upper atmosphere at EVK2-CNR. But the aerosol load at Pokhara is nearly completely influenced by the local emissions. Based on the objective phenomenon of aerosol daytime variations, we try to elucidate aerosol daytime variations in the Himalayan region. This interpretation is inferred by us, however, this results need more direct evidences such as chemical sampling at different atmosphere layers or micro-pulse lidar observations from surface. These aspects need further studies in future. However, these uncertainties or problems could be solved if some new approaches would emerge and other advanced instruments would be installed on the TP in future researches.

ACPD
13, 20961–21002, 2013

Acknowledgements. This research was funded by the Chinese National Key Programme for Developing Basic Sciences (2010CB951701), the Chinese National Natural Science Foundation (41275010 and 41275028), the EU-FP7 projects of "CORE-CLIMAX"(313085). Thanks very much for the data provided from NASA, QOMS_CAS, EVK2-CNR and Pokhara. We are grateful to Jun Qin, Yingying Chen, Xuelei Zhang for helpful discussions. Thanks for the help and advices from Hui Wu, Wenjun Tang, Menglei Han, Hongbo Zhang, Yongjie Wang, Zhongyan Wang and all the other group members.

References

Anderson, T. L., Charlson, R. J., Winker, D. M., Ogren, J. A., and Holmen, K.: Mesoscale variations of tropospheric aerosols, J. Atmos. Sci., 60, 119–136, doi:10.1175/1520-0469(2003)060<0119:mvota>2.0.co;2, 2003.

Andreae, M. O. and Merlet, P.: Emission of trace gases and aerosols from biomass burning, Global Biogeochem. Cy., 15, 955–966, doi:10.1029/2000gb001382, 2001.

Ångström, A.: On the atmospheric transmission of sun radiation and on dust in the air, Geogr. Ann., 11, 156–166, 1929.

Ångström, A.: The parameters of atmospheric turbidity, Tellus, 16, 64–75, 1964.

Barros, A. P., Joshi, M., Putkonen, J., and Burbank, D. W.: A study of the 1999 monsoon rainfall in a mountainous region in central Nepal using TRMM products and rain gauge observations, Geophys. Res. Lett., 27, 3683–3686, doi:10.1029/2000gl011827, 2000.

Bashyal, A., Majumder, A. K., and Khanal, S. N.: Quantification of PM_{10} concentration in occupation environment of traffic police personnel in Pokhara sub-metropolitan city, Nepal, Kathmandu University Journal of Science, Engineering and Technology, 4, 73–80, doi:10.3126/kuset.v4i1.2886, 2008.

Bonasoni, P., Laj, P., Angelini, F., Arduini, J., Bonafe, U., Calzolari, F., Cristofanelli, P., Decesari, S., Facchini, M. C., Fuzzi, S., Gobbi, G. P., Maione, M., Marinoni, A., Petzold, A., Roccato, F., Roger, J. C., Sellegri, K., Sprenger, M., Venzac, H., Verza, G. P., Villani, P., and Vuillermoz, E.: The ABC-Pyramid Atmospheric Research Observatory in Himalaya for aerosol, ozone and halocarbon measurements, Sci. Total. Environ., 391, 252–261, doi:10.1016/j.scitotenv.2007.10.024, 2008.

ACPD

13, 20961–21002, 2013

Bonasoni, P., Laj, P., Marinoni, A., Sprenger, M., Angelini, F., Arduini, J., Bonafè, U., Calzolari, F., Colombo, T., Decesari, S., Di Biagio, C., di Sarra, A. G., Evangelisti, F., Duchi, R., Facchini, M. C., Fuzzi, S., Gobbi, G. P., Maione, M., Panday, A., Roccato, F., Sellegri, K., Venzac, H., Verza, GP., Villani, P., Vuillermoz, E., and Cristofanelli, P.: Atmospheric Brown Clouds in the Himalayas: first two years of continuous observations at the Nepal Climate Observatory-Pyramid (5079 m), Atmos. Chem. Phys., 10, 7515–7531, doi:10.5194/acp-10-7515-2010, 2010.

Breon, F. M., Vermeulen, A., and Descloitres, J.: An evaluation of satellite aerosol products against sunphotometer measurements, Remote Sens. Environ., 115, 3102–3111, 2011.

Cao, J., Tie, X., Xu, B., Zhao, Z., Zhu, C., Li, G., and Liu, S.: Measuring and modeling black carbon (BC) contamination in the SE Tibetan Plateau, J. Atmos. Chem., 67, 45–60, doi:10.1007/s10874-011-9202-5, 2011.

Carrico, C. M., Bergin, M. H., Shrestha, A. B., Dibb, J. E., Gomes, L., and Harris, J. M.: The importance of carbon and mineral dust to seasonal aerosol properties in the Nepal Himalaya, Atmos. Environ., 37, 2811–2824, doi:10.1016/s1352-2310(03)00197-3, 2003.

Chand, D., Wood, R., Ghan, S. J., Wang, M., Ovchinnikov, M., Rasch, P. J., Miller, S., Schichtel, B., and Moore, T.: Aerosol optical depth increase in partly cloudy conditions, J. Geophys. Res.-Atmos., 117, doi:10.1029/2012jd017894, 2012.

Cong, Z., Kang, S., Smirnov, A., and Holben, B.: Aerosol optical properties at Nam Co, a remote site in central Tibetan Plateau, Atmos. Res., 92, 42–48, doi:10.1016/j.atmosres.2008.08.005, 2009.

Cong, Z. Y., Kang, S. C., Liu, X. D., and Wang, G. F.: Elemental composition of aerosol in the Nam Co region, Tibetan Plateau, during summer monsoon season, Atmos. Environ., 41, 1180–1187, doi:10.1016/j.atmosenv.2006.09.046, 2007.

Dubovik, O. and King, M. D.: A flexible inversion algorithm for retrieval of aerosol optical properties from Sun and sky radiance measurements, J. Geophys. Res.-Atmos., 105, 20673–20696, doi:10.1029/2000jd900282, 2000.

Dubovik, O., Holben, B., Eck, T. F., Smirnov, A., Kaufman, Y. J., King, M. D., Tanre, D., and Slutsker, I.: Variability of absorption and optical properties of key aerosol types observed in worldwide locations, J. Atmos. Sci., 59, 590–608, doi:10.1175/1520-0469(2002)059<0590:voaaop>2.0.co;2, 2002a.

ACPD
13, 20961–21002, 2013

Dubovik, O., Holben, B. N., Lapyonok, T., Sinyuk, A., Mishchenko, M. I., Yang, P., and Slutsker, I.: Non-spherical aerosol retrieval method employing light scattering by spheroids, Geophys. Res. Lett., 29, 54-1–54-4, doi:10.1029/2001GL014506, 2002b.

Dumka, U. C., Moorthy, K. K., Tripathi, S. N., Hegde, P., and Sagar, R.: Altitude variation of aerosol properties over the Himalayan range inferred from spatial measurements, J. Atmos. Sol.-Terr. Phy., 73, 1747–1761, doi:10.1016/j.jastp.2011.04.002, 2011.

Eck, T. F., Holben, B. N., Reid, J. S., Dubovik, O., Smirnov, A., O'Neill, N. T., Slutsker, I., and Kinne, S.: Wavelength dependence of the optical depth of biomass burning, urban, and desert dust aerosols, J. Geophys. Res.-Atmos., 104, 31333–31349, doi:10.1029/1999jd900923, 1999.

Gautam, R., Hsu, N. C., Lau, K. M., Tsay, S. C., and Kafatos, M.: Enhanced pre-monsoon warming over the Himalayan-Gangetic region from 1979 to 2007, Geophys. Res. Lett., 36, L07704, doi:10.1029/2009gl037641, 2009.

Gautam, R., Hsu, N. C., Tsay, S. C., Lau, K. M., Holben, B., Bell, S., Smirnov, A., Li, C., Hansell, R., Ji, Q., Payra, S., Aryal, D., Kayastha, R., and Kim, K. M.: Accumulation of aerosols over the Indo-Gangetic plains and southern slopes of the Himalayas: distribution, properties and radiative effects during the 2009 pre-monsoon season, Atmos. Chem. Phys., 11, 12841–12863, doi:10.5194/acp-11-12841-2011, 2011.

Gobbi, G. P., Kaufman, Y. J., Koren, I., and Eck, T. F.: Classification of aerosol properties derived from AERONET direct sun data, Atmos. Chem. Phys., 7, 453–458, doi:10.5194/acp-7-453-2007, 2007.

Gobbi, G. P., Angelini, F., Bonasoni, P., Verza, G. P., Marinoni, A., and Barnaba, F.: Sun-photometry of the 2006–2007 aerosol optical/radiative properties at the Himalayan Nepal Climate Observatory-Pyramid (5079 m a.s.l.), Atmos. Chem. Phys., 10, 11209–11221, doi:10.5194/acp-10-11209-2010, 2010.

He, Q., Li, C., Tang, X., Li, H., Geng, F., and Wu, Y.: Validation of MODIS derived aerosol optical depth over the Yangtze River Delta in China, Remote Sens. Environ., 114, 1649–1661, doi:10.1016/j.rse.2010.02.015, 2010.

He, Q., Li, C., Geng, F., Lei, Y., and Li, Y.: Study on Long-term Aerosol Distribution over the Land of East China Using MODIS Data, Aerosol Air Qual. Res., 12, 304–319, doi:10.4209/aaqr.2011.11.0200, 2012a.

ACPD
13, 20961–21002, 2013

He, Q., Li, C., Geng, F., Yang, H., Li, P., Li, T., Liu, D., and Pei, Z.: Aerosol optical properties retrieved from Sun photometer measurements over Shanghai, China, J. Geophys. Res.-Atmos., 117, D16204, doi:10.1029/2011jd017220, 2012b.
Holben, B. N., Eck, T. F., Slutsker, I., Tanre, D., Buis, J. P., Setzer, A., Vermote, E., Reagan, J. A., Kaufman, Y. J., Nakajima, T., Lavenu, F., Jankowiak, I., and Smirnov, A.: AERONET – a federated instrument network and data archive for aerosol characterization, Remote Sens. Environ., 66, 1–16, doi:10.1016/s0034-4257(98)00031-5, 1998.
Holben, B. N., Tanre, D., Smirnov, A., Eck, T. F., Slutsker, I., Abuhassan, N., Newcomb, W. W., Schafer, J. S., Chatenet, B., Lavenu, F., Kaufman, Y. J., Castle, J. V., Setzer, A., Markham, B., Clark, D., Frouin, R., Halthore, R., Karneli, A., O'Neill, N. T., Pietras, C., Pinker, R. T., Voss, K., and Zibordi, G.: An emerging ground-based aerosol climatology: aerosol optical depth from AERONET, J. Geophys. Res.-Atmos., 106, 12067–12097, doi:10.1029/2001jd900014, 2001.
Huang, J., Minnis, P., Yi, Y., Tang, Q., Wang, X., Hu, Y., Liu, Z., Ayers, K., Trepte, C., and Winker, D.: Summer dust aerosols detected from CALIPSO over the Tibetan Plateau, Geophys. Res. Lett., 34, L18805, doi:10.1029/2007gl029938, 2007.
Huffman, G. J., Adler, R. F., Bolvin, D. T., Gu, G., Nelkin, E. J., Bowman, K. P., Hong, Y., Stocker, E. F., and Wolff, D. B.: The TRMM multisatellite precipitation analysis (TMPA): quasi-global, multiyear, combined-sensor precipitation estimates at fine scales, J. Hydrometeorol., 8, 38–55, doi:10.1175/jhm560.1, 2007.
IPCC: Climate Change: The Physical Science Basis, edited by: Solomon, S., Qin, D., Manning, M., Chen, Z., Marquis, M., Avery, K. B., Tignor, M., and Miller, H. L., Cambridge University Press, Cambridge, UK and New York, NY, USA, 996 pp., 2007.
Kansakar, S. R., Hannah, D. M., Gerrard, J., and Rees, G.: Spatial pattern in the precipitation regime of Nepal, Int. J. Climatol., 24, 1645–1659, doi:10.1002/joc.1098, 2004.
Kaskaoutis, D. G. and Kambezidis, H. D.: Comparison of the Angstrom parameters retrieval in different spectral ranges with the use of different techniques, Meteorol. Atmos. Phys., 99, 233–246, doi:10.1007/s00703-007-0279-y, 2008.
Kaufman, Y. J., Tanre, D., and Boucher, O.: A satellite view of aerosols in the climate system, Nature, 419, 215–223, doi:10.1038/nature01091, 2002.
Kok, J. F.: Does the size distribution of mineral dust aerosols depend on the wind speed at emission?, Atmos. Chem. Phys., 11, 10149–10156, doi:10.5194/acp-11-10149-2011, 2011.
Koracin, D., Vellore, R., Lowenthal, D. H., Watson, J. G., Koracin, J., McCord, T., DuBois, D. W., Chen, L. W. A., Kumar, N., Knipping, E. M., Wheeler, N. J. M., Craig, K., and Reid, S.:

ACPD
13, 20961–21002, 2013

Regional source identification using Lagrangian stochastic particle dispersion and HYSPLIT backward-trajectory models, J. Air Waste Manage., 61, 660–672, doi:10.3155/1047-3289.61.6.660, 2011.

Kreuter, A., Wuttke, S., and Blumthaler, M.: Improving Langley calibrations by reducing diurnal variations of aerosol Ångström parameters, Atmos. Meas. Tech., 6, 99–103, doi:10.5194/amt-6-99-2013, 2013.

Lau, K. M., Kim, M. K., and Kim, K. M.: Asian summer monsoon anomalies induced by aerosol direct forcing: the role of the Tibetan Plateau, Clim. Dynam., 26, 855–864, doi:10.1007/s00382-006-0114-z, 2006.

Lee, J., Kim, J., Song, C. H., Kim, S. B., Chun, Y., Sohn, B. J., and Holben, B. N.: Characteristics of aerosol types from AERONET sunphotometer measurements, Atmos. Environ., 44, 3110–3117, doi:10.1016/j.atmosenv.2010.05.035, 2010.

Li, M., Ma, Y., and Zhong, L.: The Turbulence Characteristics of the Atmospheric Surface Layer on the North Slope of Mt. Everest Region in the Spring of 2005, J. Meteorol. Soc. Jpn., 90, 185–193, doi:10.2151/jmsj.2012-C13, 2012.

Li, Z. Q., Chen, H., Cribb, M., Dickerson, R., Holben, B., Li, C., Lu, D., Luo, Y., Maring, H., Shi, G., Tsay, S. C., Wang, P., Wang, Y., Xia, X., Zheng, Y., Yuan, T., and Zhao, F.: Preface to special section on east Asian studies of tropospheric aerosols: an international regional experiment (EAST-AIRE), J. Geophys. Res.-Atmos., 112, D22S00, doi:10.1029/2007jd008853, 2007.

Li, Z. Q., Li, C., Chen, H., Tsay, S. C., Holben, B., Huang, J., Li, B., Maring, H., Qian, Y., Shi, G., Xia, X., Yin, Y., Zheng, Y., and Zhuang, G.: East Asian Studies of Tropospheric Aerosols and their Impact on Regional Climate (EAST-AIRC): an overview, J. Geophys. Res.-Atmos., 116, D00K34, doi:10.1029/2010jd015257, 2011.

Liu, Z., Liu, D., Huang, J., Vaughan, M., Uno, I., Sugimoto, N., Kittaka, C., Trepte, C., Wang, Z., Hostetler, C., and Winker, D.: Airborne dust distributions over the Tibetan Plateau and surrounding areas derived from the first year of CALIPSO lidar observations, Atmos. Chem. Phys., 8, 5045–5060, doi:10.5194/acp-8-5045-2008, 2008.

Logan, T., Xi, B., Dong, X., Li, Z., and Cribb, M.: Classification and investigation of Asian aerosol absorptive properties, Atmos. Chem. Phys., 13, 2253–2265, doi:10.5194/acp-13-2253-2013, 2013.

ACPD
13, 20961–21002, 2013

Lu, Z., Streets, D. G., Zhang, Q., and Wang, S.: A novel back-trajectory analysis of the origin of black carbon transported to the Himalayas and Tibetan Plateau during 1996–2010, Geophys. Res. Lett., 39, L01809, doi:10.1029/2011gl049903, 2012.

Ma, Y., Fan, S., Ishikawa, H., Tsukamoto, O., Yao, T., Koike, T., Zuo, H., Hu, Z., and Su, Z.: Diurnal and inter-monthly variation of land surface heat fluxes over the central Tibetan Plateau area, Theor. Appl. Climatol., 80, 259–273, doi:10.1007/s00704-004-0104-1, 2005.

Ma, Y., Wang, Y., Zhong, L., Wu, R., Wang, S., and Li, M.: The characteristics of atmospheric turbulence and radiation energy transfer and the structure of atmospheric boundary layer over the northern slope area of Himalaya, J. Meteorol. Soc. Jpn., 89, 345–353, doi:10.2151/jmsj.2011-A24, 2011.

Mishra, A. K. and Shibata, T.: Synergistic analyses of optical and microphysical properties of agricultural crop residue burning aerosols over the Indo-Gangetic Basin (IGB), Atmos. Environ., 57, 205–218, doi:10.1016/j.atmosenv.2012.04.025, 2012.

Pandithurai, G., Pinker, R. T., Devara, P. C. S., Takamura, T., and Dani, K. K.: Seasonal asymmetry in diurnal variation of aerosol optical characteristics over Pune, Western India, J. Geophys. Res.-Atmos., 112, D08208, doi:10.1029/2006jd007803, 2007.

Pant, P., Hegde, P., Dumka, U. C., Sagar, R., Satheesh, S. K., Moorthy, K. K., Saha, A., and Srivastava, M. K.: Aerosol characteristics at a high-altitude location in central Himalayas: optical properties and radiative forcing, J. Geophys. Res., 111, D17206, doi:10.1029/2005jd006768, 2006.

Ramanathan, V., Crutzen, P. J., Kiehl, J. T., and Rosenfeld, D.: Aerosols, climate, and the hydrological cycle, Science, 294, 2119–2124, doi:10.1126/science.1064034, 2001.

Rehman, I. H., Ahmed, T., Praveen, P. S., Kar, A., and Ramanathan, V.: Black carbon emissions from biomass and fossil fuels in rural India, Atmos. Chem. Phys., 11, 7289–7299, doi:10.5194/acp-11-7289-2011, 2011.

Sena, E. T., Artaxo, P., and Correia, A. L.: Spatial variability of the direct radiative forcing of biomass burning aerosols and the effects of land use change in Amazonia, Atmos. Chem. Phys., 13, 1261–1275, doi:10.5194/acp-13-1261-2013, 2013.

Sharma, R. K., Bhattarai, B. K., Sapkota, B. K., Gewali, M. B., and Kjeldstad, B.: Black carbon aerosols variation in Kathmandu valley, Nepal, Atmos. Environ., 63, 282–288, doi:10.1016/j.atmosenv.2012.09.023, 2012.

ACPD
13, 20961–21002, 2013

Singh, R. P., Dey, S., Tripathi, S. N., Tare, V., and Holben, B.: Variability of aerosol parameters over Kanpur, Northern India, J. Geophys. Res.-Atmos., 109, D23206, doi:10.1029/2004jd004966, 2004.
Smirnov, A., Holben, B. N., Eck, T. F., Slutsker, I., Chatenet, B., and Pinker, R. T.: Diurnal variability of aerosol optical depth observed at AERONET (Aerosol Robotic Network) sites, Geophys. Res. Lett., 29, 2115, doi:10.1029/2002gl016305, 2002a.
Smirnov, A., Holben, B. N., Kaufman, Y. J., Dubovik, O., Eck, T. F., Slutsker, I., Pietras, C., and Halthore, R. N.: Optical properties of atmospheric aerosol in maritime environments, J. Atmos. Sci., 59, 501–523, doi:10.1175/1520-0469(2002)059<0501:opoaai>2.0.co;2, 2002b.
Sun, F., Ma, Y., Li, M., Ma, W., Tian, H., and Metzger, S.: Boundary layer effects above a Himalayan valley near Mount Everest, Geophys. Res. Lett., 34, L08808, doi:10.1029/2007gl029484, 2007.
Tosca, M. G., Randerson, J. T., Zender, C. S., Nelson, D. L., Diner, D. J., and Logan, J. A.: Dynamics of fire plumes and smoke clouds associated with peat and deforestation fires in Indonesia, J. Geophys. Res., 116, D08207, doi:10.1029/2010jd015148, 2011.
Vadrevu, K. P., Badarinath, K. V., and Anuradha, E.: Spatial patterns in vegetation fires in the Indian region, Environ. Monit. Assess., 147, 1–13, doi:10.1007/s10661-007-0092-6, 2008.
Vadrevu, K. P., Ellicott, E., Giglio, L., Badarinath, K. V. S., Vermote, E., Justice, C., and Lau, W. K. M.: Vegetation fires in the himalayan region – aerosol load, black carbon emissions and smoke plume heights, Atmos. Environ., 47, 241–251, doi:10.1016/j.atmosenv.2011.11.009, 2012.
Wang, J., Xia, X. G., Wang, P. C., and Christopher, S. A.: Diurnal variability of dust aerosol optical thickness and Angstrom exponent over dust source regions in China, Geophys. Res. Lett., 31, L08107, doi:10.1029/2004gl019580, 2004.
Wang, L., Xin, J., Wang, Y., Li, Z., Liu, G., and Li, J.: Evaluation of the MODIS aerosol optical depth retrieval over different ecosystems in China during EAST-AIRE, Atmos. Environ., 41, 7138–7149, doi:10.1016/j.atmosenv.2007.05.001, 2007.
Wild, M.: Global dimming and brightening: a review, J. Geophys. Res.-Atmos., 114, D00D16, doi:10.1029/2008jd011470, 2009.
Wu, G., Liu, Y., Wang, T., Wan, R., Liu, X., Li, W., Wang, Z., Zhang, Q., Duan, A., and Liang, X.: The influence of mechanical and thermal forcing by the Tibetan Plateau on Asian climate, J. Hydrometeorol., 8, 770–789, doi:10.1175/jhm609.1, 2007.

ACPD
13, 20961–21002, 2013

Wu, G., Liu, Y., He, B., Bao, Q., Duan, A., and Jin, F.-F.: Thermal controls on the Asian summer monsoon, Scientific Reports, 2, 404, doi:10.1038/srep00404, 2012.

Xia, X. G., Wang, P. C., Wang, Y. S., Li, Z. Q., Xin, J. Y., Liu, J., and Chen, H. B.: Aerosol optical depth over the Tibetan Plateau and its relation to aerosols over the Taklimakan Desert, Geophys. Res. Lett., 35, L16804, doi:10.1029/2008gl034981, 2008.

Xia, X. G., Zong, X. M., Cong, Z. Y., Chen, H. B., Kang, S. C., and Wang, P. C.: Baseline continental aerosol over the central Tibetan plateau and a case study of aerosol transport from South Asia, Atmos. Environ., 45, 7370–7378, 2011.

Xu, B., Cao, J., Hansen, J., Yao, T., Joswia, D. R., Wang, N., Wu, G., Wang, M., Zhao, H., Yang, W., Liu, X., and He, J.: Black soot and the survival of Tibetan glaciers, P. Natl. Acad. Sci. USA, 106, 22114–22118, doi:10.1073/pnas.0910444106, 2009.

Yanai, M. and Li, C. F.: Mechanism of heating and the boundary-layer over the Tibetan Plateau, Mon. Weather Rev., 122, 305–323, doi:10.1175/1520-0493(1994)122<0305:mohatb>2.0.co;2, 1994.

Yang, K., Ye, B., Zhou, D., Wu, B., Foken, T., Qin, J., and Zhou, Z.: Response of hydrological cycle to recent climate changes in the Tibetan Plateau, Climatic Change, 109, 517–534, doi:10.1007/s10584-011-0099-4, 2011.

Yao, T., Thompson, L., Yang, W., Yu, W., Gao, Y., Guo, X., Yang, X., Duan, K., Zhao, H., Xu, B., Pu, J., Lu, A., Xiang, Y., Kattel, D. B., and Joswiak, D.: Different glacier status with atmospheric circulations in Tibetan Plateau and surroundings, Nature Climate Change, 2, 663–667, doi:10.1038/nclimate1580, 2012.

Zhang, Y., Yu, H. B., Eck, T. F., Smirnov, A., Chin, M., Remer, L. A., Bian, H. S., Tan, Q., Levy, R., Holben, B. N., and Piazzolla, S.: Aerosol daytime variations over North and South America derived from multiyear AERONET measurements, J. Geophys. Res.-Atmos., 117, 5211–5211, 2012.

ACPD
13, 20961–21002, 2013

Table 1. The basic information of all the three AERONET sites (QOMS_CAS, EVK2-CNR and Pokhara) includes longitude, latitude, elevation, and date ranges of level 1.5 and level 2.0 data.

Site Name	Longitude	Latitude	Elevation (m) a.s.l.	Level 1.5 Date range	Level 2.0 Date range
QOMS_CAS	86.95° E	28.37° N	4276	Oct 2009–Jul 2010; Nov 2011–Dec 2012	Oct 2010–Oct 2011
EVK2-CNR	86.81° E	27.96° N	5050	Nov 2011–Oct 2012	Mar 2006–May 2011
Pokhara	83.97° E	28.15° N	807	Jul 2011–Dec 2012	Jan 2010–Jun 2011

ACPD
13, 20961–21002, 2013

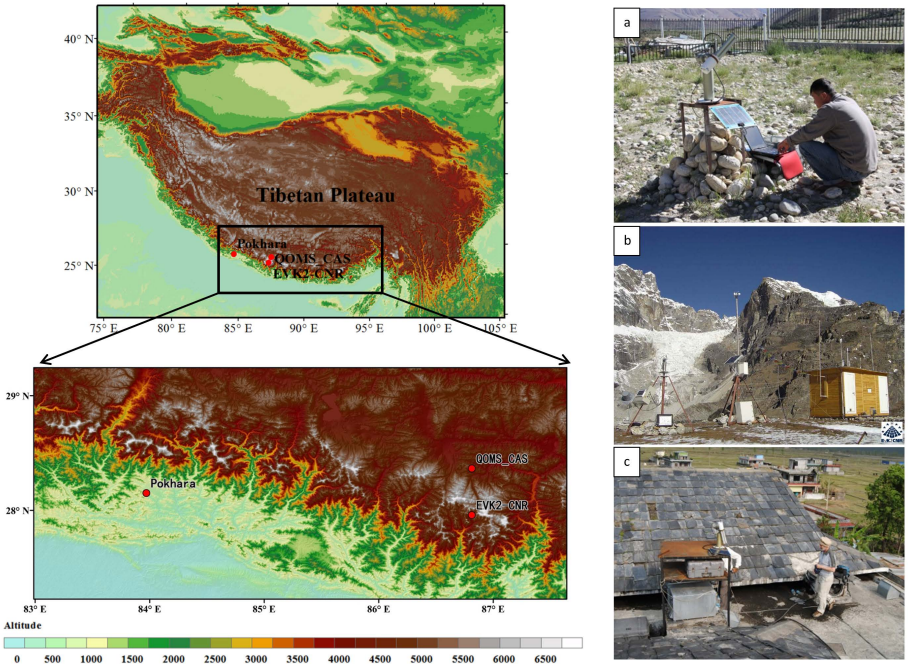

Fig. 1. The left pictures display the topography (in m) map over the Tibetan Plateau and the locations of the three AERONET sites selected for this study. The right pictures show the AERONET sunphotometer deployments in the field observations (**a** QOMS_CAS, **b** EVK2-CNR, **c**: Pokhara).

ACPD
13, 20961–21002, 2013

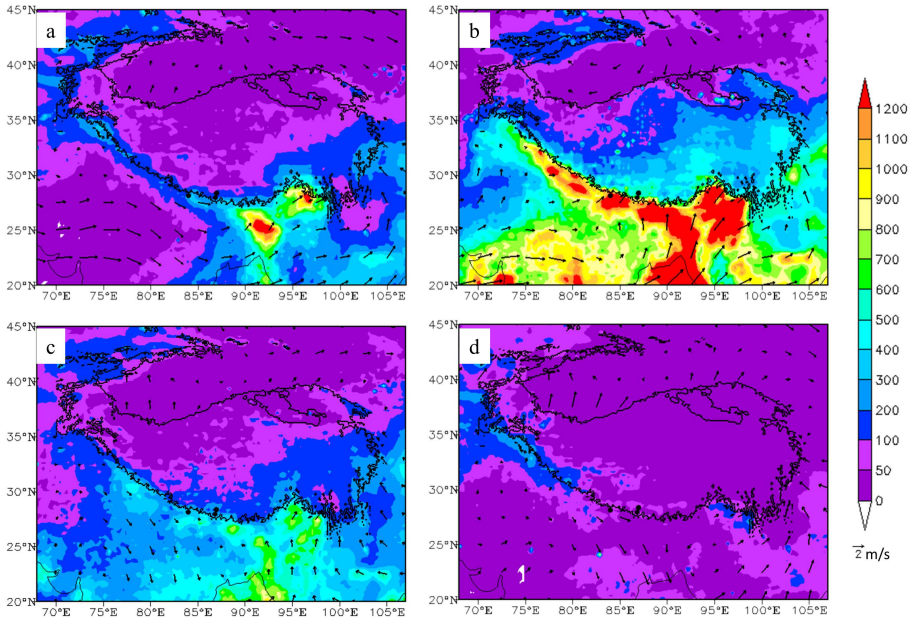

Fig. 2. Spatial distribution of TRMM-derived seasonal mean climatology of accumulated precipitation (mm) and wind at 850 hPa over the Tibetan Plateau (**a** March–May (MAM); **b** June–August (JJA); **c** September–November (SON); **d** December–February (DJF)). Bold black line marks the geographic location of Tibetan Plateau, and the black dots indicate the locations of the three station.

ACPD
13, 20961–21002, 2013

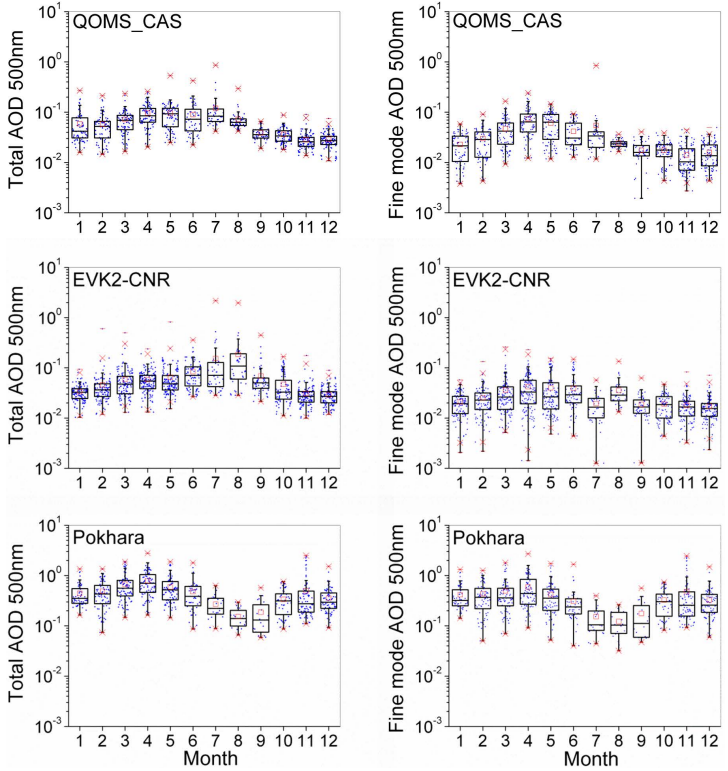

Fig. 3. Box plots of total aerosol optical depth (left) and fine mode aerosol optical depth (right) at 500 nm at QOMS_CAS, EVK2-CNR and Pokhara. The blue dots represent daily observations. The central bar is the median, and the lower and upper limits are the first and the third quartiles, respectively. The 99 % and 1 % percentile are indicated by red crosses. The maximum and minimum values are shown by red dashes. The red hollow-block symbols indicate geometric means (the following symbols are the same).

ACPD
13, 20961–21002, 2013

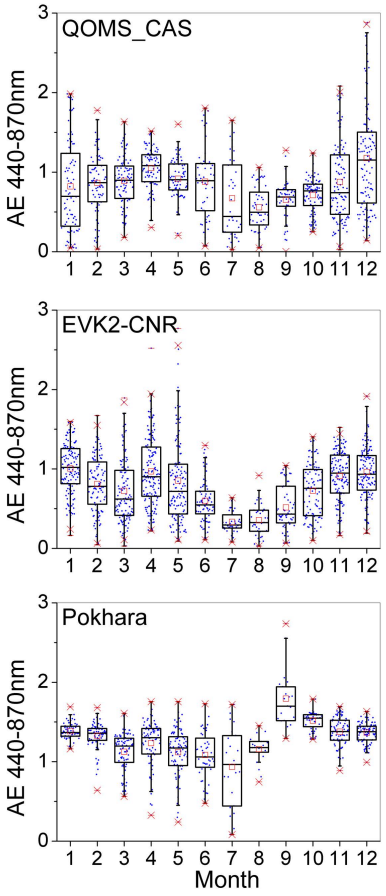

Fig. 4. Box plots of Ångström exponent at 440–870 nm at QOMS_CAS, EVK2-CNR and Pokhara. Same symbols are used as in Fig. 3.

ACPD
13, 20961–21002, 2013

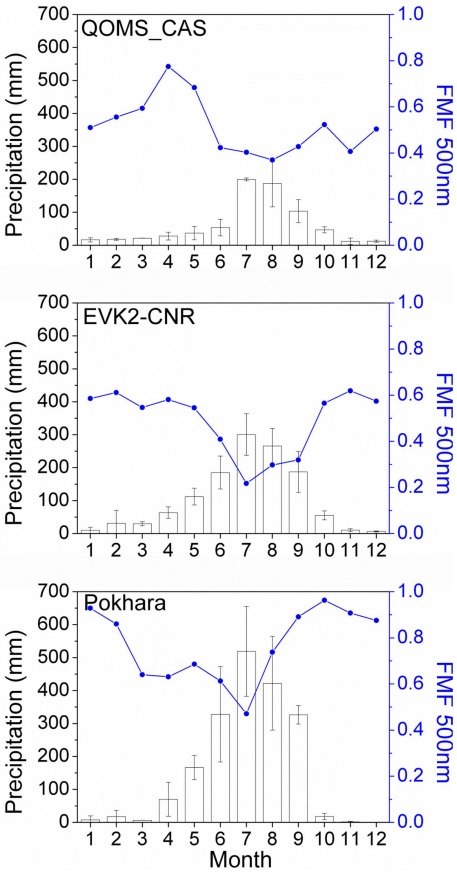

Fig. 5. Monthly means of accumulated precipitation (mm) and fine mode fraction (FMF). The uncertainty of precipitation indicates the inter-annual difference.

ACPD
13, 20961–21002, 2013

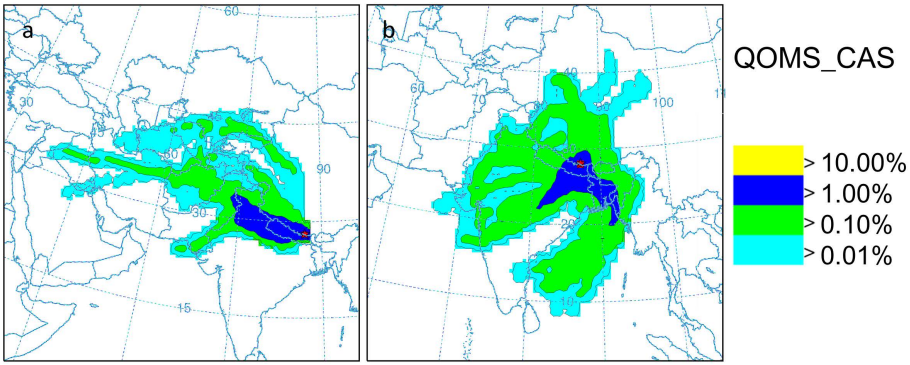

Fig. 6. Frequency plots of five-day back trajectories by using HYSPLIT at QOMS_CAS (**a** April 2012; **b** July 2012). Different colours indicate the possibility for aerosol source region.

ACPD
13, 20961–21002, 2013

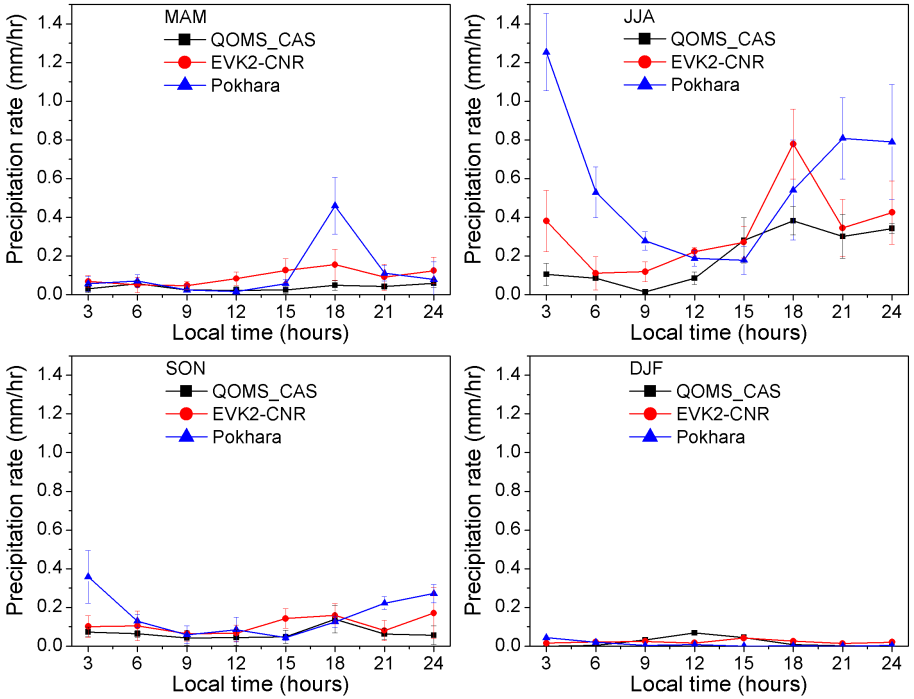

Fig. 7. Diurnal variations of PR at the three stations in all seasons. The uncertainty indicates the inter-annual difference of PR at each time. MAM denotes March to May, JJA denotes June to August, SON denotes September to November and DJF denotes December to February in the next year (the followings are the same).

ACPD
13, 20961–21002, 2013

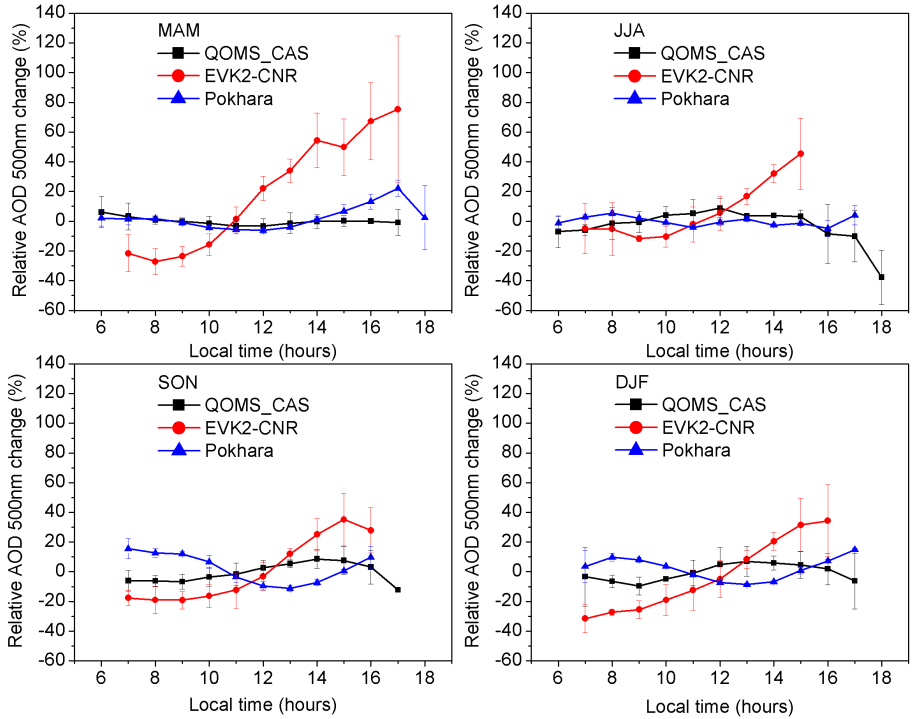

Fig. 8. Percentage deviations of hourly average AOD at 500 nm relative to their daily mean in all seasons at QOMS_CAS, EVK2-CNR and Pokhara. The uncertainty indicates the inter-annual difference of relative AOD at each hour.

ACPD
13, 20961–21002, 2013

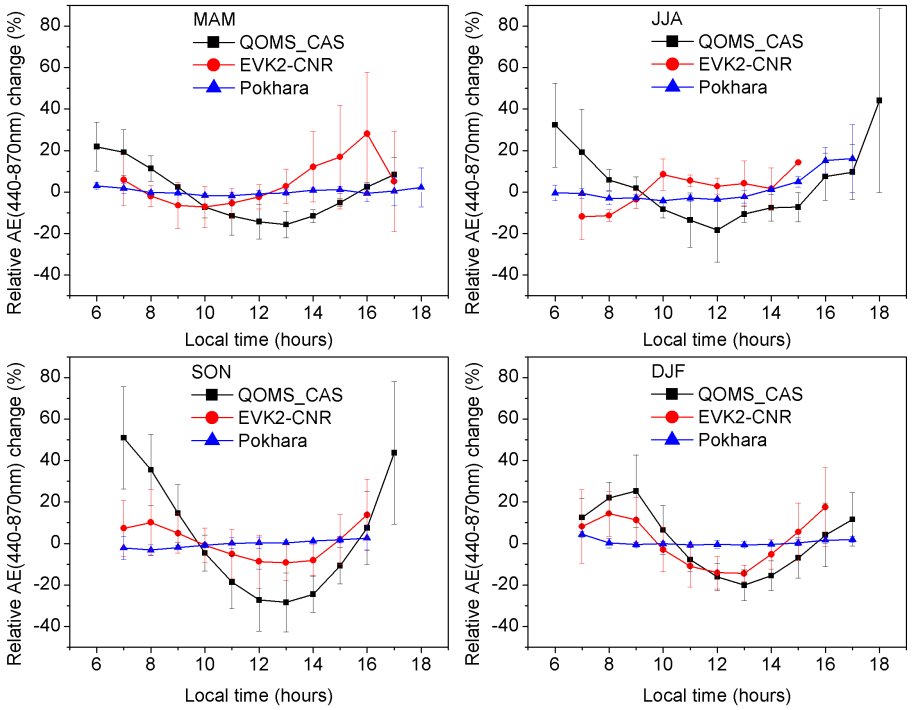

Fig. 9. Percentage deviations of hourly average AE at 440–870 nm relative to their daily mean in all seasons at QOMS_CAS, EVK2-CNR and Pokhara. The uncertainty indicates the inter-annual difference of relative AE at each hour.

ACPD
13, 20961–21002, 2013